Controlling the ionization and recombination rates of an electron in preexcited ions to generate an intense isolated sub-4-as pulse in a multicycle regime

M. Mohebbi*

Department of Physics, Faculty of Science, Vali-e-Asr University of Rafsanjan, P.O. Box 77139-36417, Rafsanjan, Iran

(Received 26 September 2014; published 27 February 2015; corrected 26 October 2021)

We present a numerical study of an isolated attosecond pulse generation in a preexcited medium driven by a moderately intense multicycle laser pulse, which is synthesized by adding a chirp-free laser pulse to a chirped laser pulse. The results show that by preparing the initial state of He^+ ion as a preexcited state, the electron trajectories significantly can be modulated and the supercontinuous harmonics with higher emission efficiency can be obtained. Optimizing the chirp parameter allows a multicycle field to behave like a few-cycle one due to the control of electron tunneling. Therefore, a wide 1172-eV intense supercontinuum would be achieved on the high-order-harmonic generation spectrum. The classical and time-frequency approaches reveal that the long quantum path is suppressed and only the short quantum path is left. By properly filtering the harmonics from the supercontinuum, a 34-as intense isolated pulse with clean time profile is directly obtained without any phase compensation. Our simulation shows that by superposing the total supercontinuum region with phase compensation, we can obtain the shortest sub-4-as intense isolated pulse.

DOI: 10.1103/PhysRevA.91.023835 PACS number(s): 42.65.Ky, 33.80.Wz, 42.65.Re, 32.80.Wr

I. INTRODUCTION

The generation of extreme-ultraviolet attosecond pulses has been established as a key tool in time-resolved investigations with high precision [1–7]. To date, high-order-harmonic generation (HHG) is the most promising route to generate the attosecond pulses, which is the result of the interaction between a strong laser pulse and an atomic or molecular system [8–11]. Generally speaking, a typical HHG spectrum shows a rapid decrease for the first few harmonics, followed by a broad plateau of almost constant conversion efficiency, ending up with a sharp cutoff at a well-known frequency of $I_p + 3.17U_p$, where I_p is the atomic ionization potential and U_p is the ponderomotive energy which only depends on the parameters of the laser field. This mechanism of HHG can be well understood in terms of a semiclassical model [12] and the quantum model [13]. According to the well-known semiclassical theory, a HHG process in gas mainly includes three steps: (1) tunnel ionization of the most weakly bound electron near the local peak of the electric field, (2) acceleration of the electron first away from its parent ion and then back by the time-varying laser field, and (3) recombination of the continuum electron into the bound electronic state and the emission of HHG radiation with energy equal to the ionization potential plus the kinetic energy of the recombining electron gained during its acceleration in the laser electric field. Each time this recombination occurs, a burst of attosecond-duration x-rays is emitted. This burst usually happens twice during each cycle of the driving laser field. To generate an isolated attosecond pulse, the emission time of the harmonics should be confined in one half cycle. By manipulating the different steps of this dynamical process, one can control HHG to generate the isolated attosecond pulse or enhance the harmonic efficiency. It has been demonstrated by Paul *et al.* that an attosecond train can be produced with a multicycle laser pulse by HHG [7]. However, straightforward attosecond metrology prefers an isolated attosecond pulse for detecting and controlling the electronic dynamics [14]; therefore, much effort has been paid to extracting such ultrashort pulses and has shown that an isolated attosecond pulse can be produced using a few-cycle driving pulse technique [15], a two-color laser technique [16], a chirped laser pulse technique [17–21], and a polarization gating technique [22,23]. Producing attosecond pulses in the above techniques is very challenging since the harmonics efficiency is low. Hence, a lot of effort has been devoted to generate higher conversion efficiency of HHG. For example, it has been suggested that the conversion efficiency of HHG can be meaningfully enhanced by proper application of an additional harmonics to populate the excited states [24]. This harmonic pulse plays a fundamental role in the transition to excited states or to a nearby virtual state. Avetissian *et al.* proposed the efficient generation of moderately high harmonics by bound-bound transitions [25–27]. Another fascinating way to produce a plateau with high energy and high conversion efficiency is to prepare a coherent superposition state of two bound states [28–31]. In this way, part of the electron wave packet in an initial state populates an excited bound state. Many ways were suggested for a population transfer from an initial state to a bound state. It can be obtained by using one harmonic pulse whose photon energy is close to the transition energy two bound states before the fundamental laser pulse [32] or adiabatic transition from a single ground state to a superposition of excited states [33–36], and excitation of multiphoton resonant excitation [25–27]. On the other hand, Wang *et al.* have studied the pulse-duration dependence of HHG and concluded that for long laser pulses, each half a laser cycle emits a short burst of radiation due to the scatter off the core of the continuum wave packet [37]. As a result, the multicycle accumulation of the harmonic generation causes separate sharp peaks in each odd harmonic order. To generate the intense continuum, Hong *et al.* advised a mechanism to generate harmonics with very high frequencies and the isolated attosecond pulse when an intense 4-fs few-cycle laser interacts with a preexcited medium [38]. Thus, it seems that by a reduction in the pulse duration of the incidence pulse, the intense

*m.mohebbi@vru.ac.ir

continuum can be obtained in a preexcited medium. However, these schemes strongly rely on the stabilization of the carrier envelope phase (CEP) of local fields. Luo *et al.* investigated the isolated attosecond pulse emission from a preexcited medium driven by noncarrier-envelope phase-stabilized nanoplasmonic fields [39]. In this paper, we propose a scheme to achieve ultrashort, ultraintense isolated attosecond pulse generation in the multicycle regime. In the single-atom response level, we investigate the manipulation of the ionization process from the He ion by using a coherent superposition of two bound states, which effectively controls HHG and generates an efficient broadband continuum in a synthesized field by a multicycle chirped laser pulse and a chirp-free laser pulse. It is shown that when the initial state is prepared as the coherent superposition state, the generated harmonic spectrum is significantly enhanced by about six orders of magnitude and an intense sub-50-as isolated attosecond pulse with a high signal-to-noise ratio is efficiently obtained. By optimizing the chirp rate of the one field, the shape of the multicycle field can be controlled to induce the change of the laser sign to one successive time. It is found that the electron ionization dynamics can be controlled to generate an intense sub-4-as isolated attosecond pulse. This would provide an efficient route to generate broadband isolated attosecond pulses without CEP stabilization. This paper is organized as follows. In Sec. II, we present the physical model to study the HHG process. In Sec. III, we show how an intense isolated attosecond laser pulse is generated when the initial state is prepared as the coherent superposition state by a synthesized field. Finally, in Sec. IV, we give the conclusions. Atomic units (a.u.) are used throughout unless otherwise indicated.

II. THEORETICAL FRAMEWORK

To verify our scheme, we investigate the HHG and the attosecond pulse generation by numerically solving the one-dimensional (1D) time-dependent Schrodinger equation with the splitting operator method. We choose a soft-core Coulomb potential model $V(z) = -\frac{a}{\sqrt{b+z^2}}$ and set $a = 2$ and $b = 0.5$ in order to get the same ground-state binding energy of a real He^+ ion, i.e., 2.000 a.u. Also, in this one-dimensional case, the binding energy of the considered excited state is 0.533 a.u. The ions were used to extend the HHG spectrum cutoff. It has been reported in several works [28,32,40,41]. Whereas the study of the hydrogenlike system is simple and accurate, the He^+ ion is chosen as a target system. Moreover, He^+ ions are experimentally more friendly since they can easily be produced, e.g., through single-photon ionization of He by 27th harmonics [32,42]. The initial state of the preexcited system can be written as

$$\Psi(z,t_0) = \frac{1}{\sqrt{2}}(|g\rangle + |e\rangle), \tag{1}$$

where $|g\rangle$ and $|e\rangle$ are the ground and excited states of the He^+ ions, respectively. Once the time evolution of the wave function $\Psi(z,t)$ is determined, the time-dependent induced dipole acceleration can be given by means of Ehrenfest's theorem [29],

$$f(t) = E(t) - \langle\Psi(z,t)|\frac{\partial V}{\partial z}|\Psi(z,t)\rangle, \tag{2}$$

and the HHG power spectrum can be determined, which is proportional to the modulus squared of the Fourier transform of $f(t)$. It is given by

$$P(\omega) = \left|\frac{1}{\sqrt{2\pi}}\int_0^t f(t)e^{-i\omega t}dt\right|^2. \tag{3}$$

To analyze the temporal structures of HHG, we perform the time-frequency analysis by means of the wavelet transform [43],

$$f_\omega(t) = \int_0^t f(\acute{t})\sqrt{\omega}W[\omega(t-\acute{t})]d\acute{t}, \tag{4}$$

where $W[\omega(t-\acute{t})]$ is the mother wavelet. A natural choice of the mother wavelet is given by the Morlet wavelet,

$$W(y) = \frac{1}{\sqrt{\alpha}}e^{-\frac{y^2}{2\alpha^2}+iy}. \tag{5}$$

In the present work, we choose $\alpha = 15$ to perform the wavelet transform. By superposing several harmonics, an ultrashort pulse can be generated,

$$I(t) = \left|\sum_q f_q e^{+iq\omega t}\right|^2, \tag{6}$$

where $f_q = \int f(t)e^{-iq\omega t}dt$. The time-dependent ionization probability is defined as $P_{\rm ion}(t) = 1 - \sum_n |\langle n|\Psi\rangle|^2$, where the summation runs over the bound states $|n\rangle$. In our simulation, the laser field is along the z axis and can be expressed in the form

$$E(t) = E_0 f(t)\{\cos[\omega_0 t + \phi(t)] + \cos(\omega_0 t + \varphi)\}, \tag{7}$$

where E_0 is the laser field amplitude, $f(t) = e^{-4Ln2(t^2/\tau^2)}$ is the laser field envelope, $\omega_0 = 0.057$, and $\tau = 372$ [full width at half maximum(FWHM)] are the corresponding frequency and duration, respectively. φ is the relative phase and $\phi(t)$ is the carrier-envelope phase (CEP) [44], which has the time-varying form $\phi(t) = -\beta\omega_0 t^2/\tau_0$. β and τ_0 are employed to control the chirp form. In our work, we fix τ_0 to be 10 optical cycles (o.c.), i.e., the length of time for the time evolution, while the parameter β varies. Currently, a 9-fs, 800-nm laser pulse (Ti:sapphire) is available in a few good laboratories. This form of frequency-chirped pulses has already been employed experimentally [45,46]. To understand the physics behind the dynamic of HHG, the three-step simulation is performed [12]. If an electron is ionized at t_i, the corresponding emission time t_e can be obtained by solving the following equation:

$$\int_{t_i}^{t_e} dt \int_{t_i}^{t} E(t)dt = 0. \tag{8}$$

The kinetic energy E_k of an electron ionized at t_i and returning to the parent ion at t_e can simply be expressed as

$$E_k = \frac{1}{2}\left[\int_{t_i}^{t_e} E(t)dt\right]^2. \tag{9}$$

By solving Eqs. (8) and (9), we can investigate the electronic dynamics of the HHG process in the synthesized field.

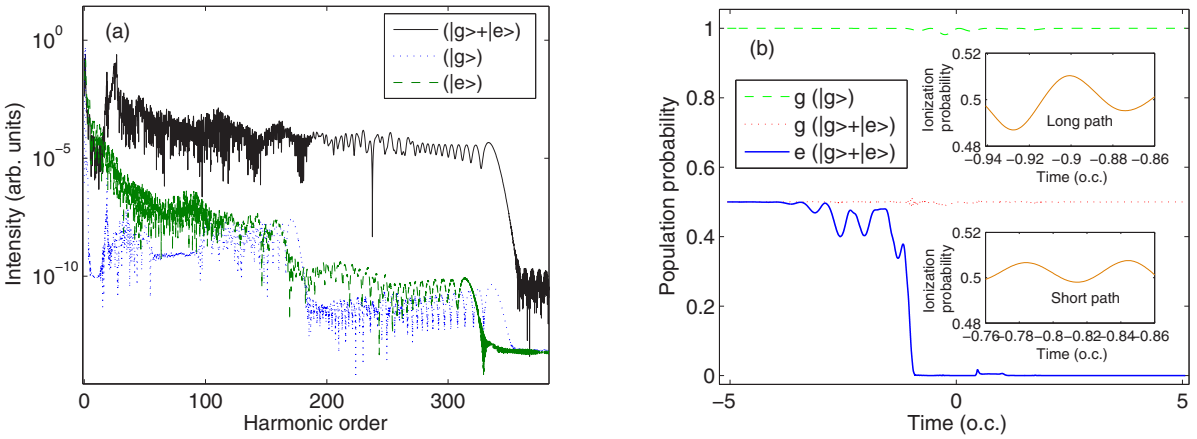

FIG. 1. (Color online) (a) Harmonic spectra from He^+ ions initially prepared in the coherent superposition of the ground and excited states irradiated by a synthesized field of a 9-fs, 800-nm ($\beta = 0.58$) and a 9-fs, 800-nm laser pulse (solid black curve). The dotted blue and dashed green curves show harmonic spectra from He^+ ions initially prepared in the ground and excited states, respectively, irradiated by this field. The intensities of the pulses are 4×10^{14} and 4×10^{14} W/cm^2. The relative phase φ is set to zero. (b) Population probabilities of the ground (dotted red curve) and excited (solid blue curve) states as a function of time when the initial state is a coherent superposition of the ground and excited states. The upper and lower insets show the long and short classical-path ionization probabilities. The dashed green curve shows the population probability of the ground state from He^+ ions initially prepared in the ground state.

III. RESULT AND DISCUSSION

First, we investigate the HHG of He^+ ions initially prepared in the ground state when they are exposed to a laser field synthesized by the 9-fs, 800-nm chirped pulse with arbitrary value of $\beta = 0.58$ and the 9-fs, 800-nm chirp-free pulse. The peak intensity I_0 is 4×10^{14} W/cm^2 (corresponding to the electric-field amplitude $E_0 = 0.106$ a.u.). By selecting the relative phase $\varphi = 0$ between the two lasers, the harmonic spectrum shows a structure with two plateaus, as shown by the dotted blue curve in Fig. 1(a). The two cutoff positions of the spectrum are the 174th and the 336th order. As demonstrated in Fig. 1(a), the height of the second plateau is lower than the first one. Furthermore, one can clearly see that the harmonic spectrum is regular and continuous in the first plateau (near the cutoff) and the second one. Note that the harmonic efficiency is extremely low due to the He^+ ions, large ionization potential.

The dashed green curve in Fig. 1(b) exhibits the population probability as a function of time when the initial state is prepared as the ground state. The ionization probability of He^+ ions from the ground state is too weak due to the laser-pulse intensity in our simulation being much lower than the saturation intensity of He^+ (i.e., a moderately intense pulse). According to the semiclassical HHG model, the conversion efficiency of the plateau harmonic is directly proportional to the ionization rate (i.e., population of the continuum states) and remaining bound population (i.e., the ground-state population). Despite the large amount of the ground-state population, the harmonic signal for ions has been shown to be very weak because the ionization rate is very low. As pointed out by Mohebbi *et al.*, the dipole transition is induced between the continuum and the ground state, where only the ground state is responsible for the ionization which is directly proportional to the ionization rate [31]. If we use the rare-gas atoms, the large ionization of the ground state populates the continuum while depleting the ground state. As a result, the conversion efficiency is decreased. This suggests that a high efficiency of the harmonic signal could be obtained if both the ground and continuum states have the large populations [31]. We are interested in producing high-energy-harmonic photons with high conversion efficiency. It is well known that an electron in an excited state is easier to be ionized than in the ground state. On the other hand, it is much easier to promote electrons into the continuum from the excited states. Thus, a suitable method of enhancing the harmonic efficiency is to employ an excited state in the preexcited scheme [31]. Figure 1(b) shows the population probabilities of the ground and excited states as a function of time when the initial state is a coherent superposition of the ground and excited states with equal population of 0.5. The population of the ground state approximately remains invariant at this value of intensity, as shown by the dotted red curve in Fig. 1(b) (similar to ions initially prepared in the ground state, i.e., the dashed green curve). In contrast, the population of the excited state decreases significantly, as shown by the solid blue curve in Fig. 1(b). The laser intensity is high enough to ionize the excited state within a few optical cycles, while it is too weak to directly ionize the ground state. These results testify that the total ionization probability of ion is mainly affected by large ionization of the excited state when the initial state is a coherent superposition of the ground and excited states. It increases the continuum population. The main advantage of using a coherent superposition state is that it is a suitable way to increase the harmonic conversion efficiency so that the dipole transitions can be induced between the continuum and the bound ground and excited states, where the excited state is responsible for the ionization and population of the continuum states, as shown by the solid black curve in Fig. 1(a). Thus, it is not possible to obtain the intense higher-energy harmonics with He^+ ions in a ground state alone [37,47] or with He^+ ions in an excited state alone (i.e., when the initial state is prepared as the excited state). For comparison, we also present results when the initial state is the excited state [green dashed curve

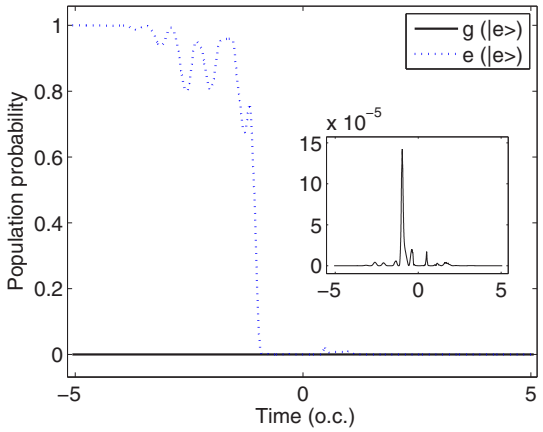

FIG. 2. (Color online) The population probability of the ground and excited states as a function of time when He^+ ions are initially prepared in the excited state with the black solid and blue dotted curves, respectively, with the same synthesized laser field (the population probability of the ground state has been enlarged in the inset).

in Fig. 1(a)]. The HHG spectrum of the excited state shows two different sets of harmonics. The second one is about one order of magnitude higher than that of the ground-state case (dotted blue curve), while it is about five orders of magnitude lower than that of the superposition states case (solid black curve). As shown in Fig. 2, the population of the excited state decreases significantly within two optical cycles (blue dotted curve). The main difficulty for He^+ in the excited state alone arises from this fact that the population of the ground state is very small (black solid curve). In the rare-gas scheme, we can hardly control both the ground-state population and depletion. But in the ion scheme, by fixing the population of the ground state at this range of pulse intensity (i.e., moderate intensity), we can easily control the excited-state depletion to generate the intense attosecond pulse. From Fig. 1(a), we can see clearly that the spectral structure of the solid black curve is not the same as that for the dotted blue curve. Indeed, we note that the height of different harmonics in the second plateau is nearly uniform and decreases only about one order of magnitude from the first plateau to the second one (solid black curve). One can notice that the position of the second cutoff in the superposition case is the same as that for the ground-state case (H336). The intensity of the second plateau in the superposition case is about seven orders higher than that of the ground-state case and a broadband supercontinuum obtained from 190th order to 336th order (i.e., 146 orders) in the second plateau. On the other hand, it is possible to use the high-efficiency continuous spectrum which was shown in the solid black curve to obtain an intense attosecond pulse. Next, we investigate the attosecond pulse generation. The temporal profile of the attosecond pulse can be produced by simply making an inverse Fourier transformation of the HHG spectrum. Figure 3(a) shows the temporal profiles of the attosecond pulses which is generated from He^+ initially in the ground state. By superposing the harmonics from 270th order to 320th order (approximately corresponds to the bandwidth of about 78 eV) in the second plateau, a regular attosecond pulse train with two bursts is observed [solid green curve in Fig. 3(a)]. The durations of the two attosecond bursts are 59 as and 21 as, and the intensity of the 59-as pulse is stronger than that of the 21-as pulse. As shown by the dashed blue curve in Fig. 3(a), an intense isolated 303-as pulse can be generated by superposing the harmonics from the 163rd order to the 180th order near the first cutoff (H174). The intensity of the 303-as pulse is stronger than that of the attosecond pulse train. In addition, by properly selecting harmonics from the 235th to 285th order (dotted red curve), one can see clearly that an intense isolated 107-as pulse with some satellite pulses around it is straightforwardly obtained without any phase compensation. Selecting the whole attainable spectral range no longer supplies the shortest pulses due to the temporal shift in harmonic emission, as reported in [48,49]. Figure 3(b) shows the temporal profiles of the generated attosecond pulses by the harmonics with different central frequencies when the initial state is a coherent superposition of the ground and excited states. As shown in this figure, by adding a frequency window with a bandwidth of 50 harmonics (77 eV) to the supercontinuum, nearly isolated attosecond pulses with some weak satellite pulses are generated. Although there are still two main bursts between -0.4 optical cycles (o.c.) and 0.4 o.c., where the optical cycle (2.67 fs) is the period of the 800-nm driving laser pulse, the intensities of the earlier bursts are very weak and ignorable. By decreasing the harmonic order, the separation between the emission times of the bursts becomes larger. As shown in this figure, the strong burst will be enhanced when we intend to superpose the harmonics with central frequencies from the 305th to 200th order. This is because the long trajectory enhances, and the efficiency of the harmonic spectrum increases effectively. This leads to a reduction of the modulation depth at these harmonics. The duration of the isolated attosecond pulse shortens slightly with the decrease of central frequency, though the intensity increases. So in a wide range of harmonics, we can obtain a short isolated attosecond pulse. By properly filtering the harmonics from the 235th to 285th order, an intense isolated pulse of 49 as (the shortest pulse duration) with a weak satellite pulse has been straightforwardly obtained without any phase compensation, as shown in Fig. 4(a). Moreover, one can see that the temporal profiles of the obtained intense attosecond pulse have high signal-to-noise ratio. It also reveals that the case of the superposition state significantly shortens the duration of the isolated attosecond pulse [Figs. 3(a) and 4(a)] and enhances the pulse intensity by about five orders of magnitude compared to the case of the ground state [dotted red curve in Fig. 3(a)]. In order to investigate the physical mechanisms underlying the formation of the supercontinuum in detail, we perform the semiclassical three-step model and calculate the ionization probability in the synthesized field with $\beta = 0.58$. The ionization probabilities of classical paths (trajectories) as a function of the time are shown by the solid curves in the insets of Fig. 1(b) when the initial state is prepared as the coherent superposition state. The kinetic-energy map in Fig. 4(b) presents the dependence of the harmonic order on the ionization (blue circles) and emission times [red plus signs (+)] in the synthesized laser field (solid black curve). We can obviously see that there are three main peaks of A, B, and C with the maximal harmonic orders of 174, 336, and

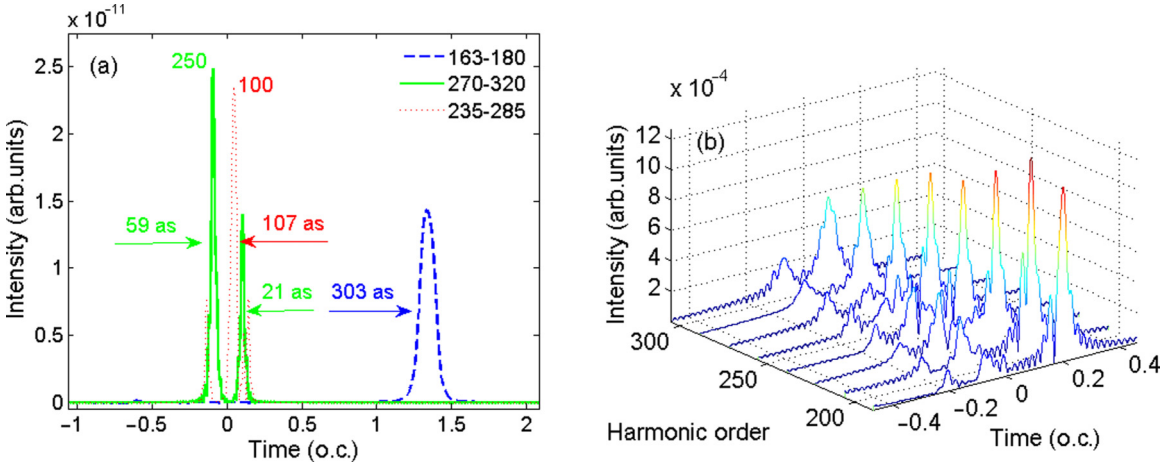

FIG. 3. (Color online) (a) The temporal profiles of the attosecond pulses from He^+ ions in the ground state: by superposing the harmonics from the 235th to 285th order (dotted red curve), from the 163rd to 180th order (dashed blue curve), and from the 270th to 320th order (solid green curve). The curves have been multiplied by factors of 1 (dashed blue curve), 250 (solid green curve), and 100 (dotted red curve), for the purpose of clarity. (b) Temporal profiles of the attosecond pulses from He^+ ions in the coherent superposition state by the harmonics with different central frequencies. The laser parameters are the same as in Fig. 1.

171, respectively, due to the ionization of electrons near the peaks of the combined laser field, which are marked as $\acute{A}$, $\acute{B}$, and $\acute{C}$, respectively. There are only two trajectories which contribute to the harmonics between the B and C peaks. Peak A is much less intense, since the laser field is weaker at the ionization time for peak $\acute{A}$ than that for peak $\acute{C}$, as shown in Fig. 4(b), leading to a smaller tunneling ionization rate. Thus, the contribution from peak A is hidden by those from peaks B and C for the case of the ground state. However, it is quite the opposite for the case of the coherent superposition state because the tunneling ionization rate of the excited state is stronger for the laser field peak $\acute{A}$ than for the laser field peak $\acute{C}$ (the intensity is higher than the saturation intensity in peak $\acute{C}$ and thus the excited state completely depletes), as can be seen from the population probability of the excited state in Fig. 1(b). Thus, the contribution of peak C is hidden by peaks A and B for the case of the coherent superposition state. Therefore, the irregular spectra structure in Fig. 1(a) at the harmonics below 171st and 174th are due to a destructive interference between peaks C and B (C-B), and A and B (A-B), for the dotted blue and solid black curves, respectively. One can see that two trajectories contribute to the harmonics between the A and B peaks for the case of the coherent superposition state, as shown in Fig. 4(b). This continuous harmonics mainly originates from the electrons ionized in the time range from -0.754 to -0.947 o.c. Electrons with the short trajectories are mainly ionized from -0.863 to -0.754 o.c. and electrons with the long trajectories are mainly ionized from -0.947 to -0.863 o.c. Near the field peak $\acute{B}$, the ionization rate for the long trajectory is higher than that for the short trajectory, which can be found from the curves in the insets of Fig. 1(b). Therefore, the harmonic efficiency for the long trajectory is mainly higher than that for the short trajectory, which causes the generation of the continuous harmonic spectrum, as shown

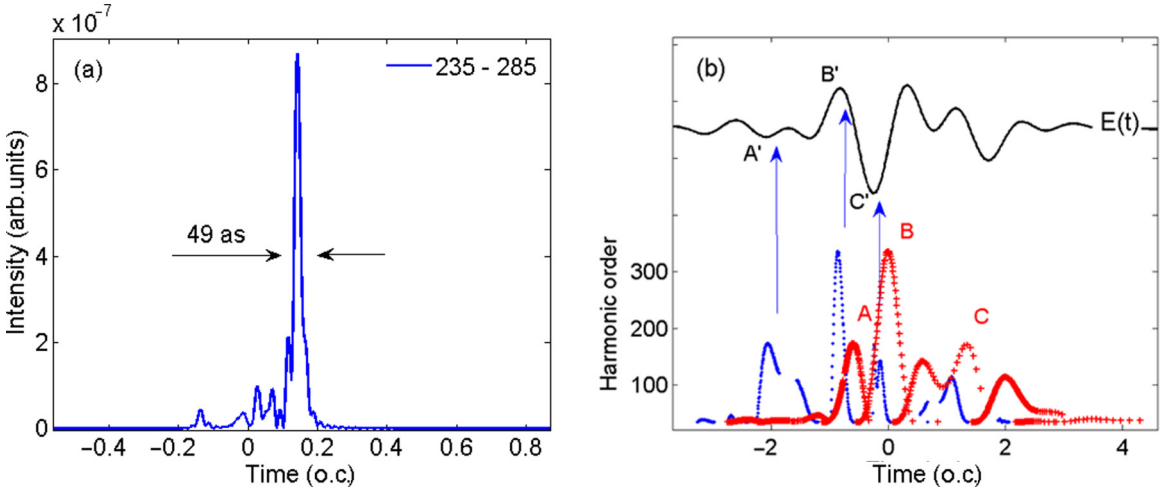

FIG. 4. (Color online) (a) The temporal profile of the attosecond pulse from He^+ ions in the coherent superposition state by superposing the harmonics from the 186th to 239th order. (b) Dependence of harmonic order on the ionization time (blue circles) and the emission time (red plus signs) in the synthesized laser field (solid black curve). The laser parameters are the same as in Fig. 1.

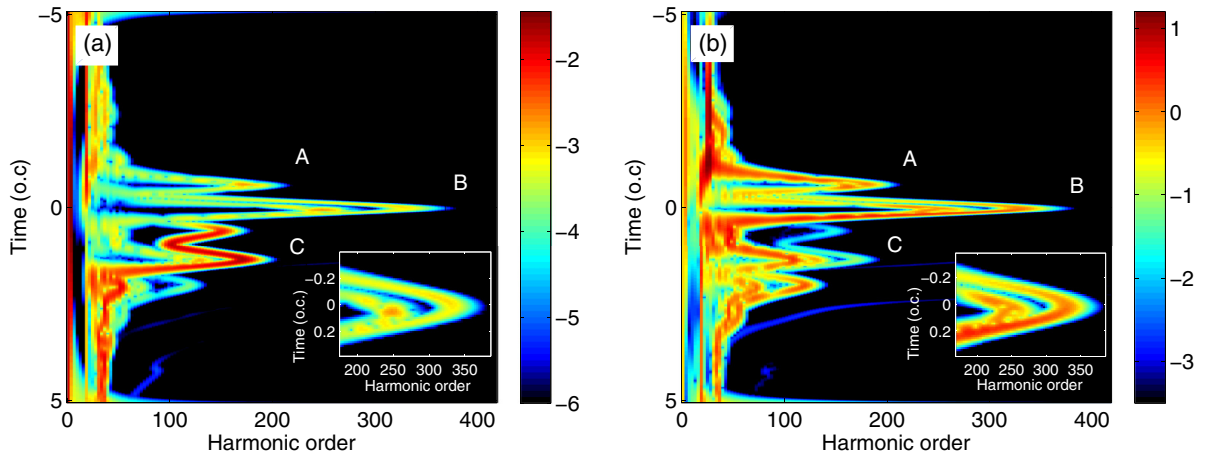

FIG. 5. (Color online) Time-frequency distributions of HHG corresponding to the (a) dotted blue and (b) solid black curves in Fig. 1. Insets: A detailed view of short and long trajectories near the cutoff. The color bar shows the high-harmonic yield in a logarithmic scale.

by the solid black curve in Fig. 1(a). These results are in agreement with the temporal profile in Fig. 3(b), in which the peak intensity of the earlier burst is weaker than that of the following burst. It is noteworthy that the ionization rates ratio increases rapidly with decreasing of the harmonic order. On the other hand, the contribution of the short trajectory is almost constant and the contribution of the long trajectory increases rapidly with the decrease of harmonic order. This result is consistent with the enhancement of the pulse intensity of about two times, as shown in Fig. 3(b). In addition, we investigate the HHG process by the quantum time-frequency analysis when the initial state of the He^+ ion is prepared in the ground state and the coherent superposition of the ground and excited states. We first consider the case of the $\beta = 0.58$ when the initial state is prepared in the ground state. As shown in Fig. 5(a), there are three photon-energy peaks, which are labeled as A, B, and C. The three peaks state the recombination times as well as the maximum kinetic energy of the electrons that return to their parent ions. The maximum harmonic orders of A, B, and C are about 174, 336, and 141, respectively, as we saw before.

We can also see a main peak C where the harmonic orders are greater than 174th over the tops of all the adjacent peaks. The dark red regions (in color scale) as seen in Fig. 5(a) indicate a significantly larger number of quantum paths than those of other regions. Thus, A and B have comparable intensity, and A (and B) is weaker than C and its contribution to the HHG can be ignored. There are two dominant quantum paths of electron (so-called short and long quantum paths) with different emission times contributing to each harmonic in the range of the main peak. The negative-slope and positive-slope branches of the main peak correspond to the short and long quantum paths, respectively. The interference between these short and long quantum paths which have the same intensity (height) will create a regular modulation in the spectrum of the supercontinuum in the second plateau. This is useful for producing an attosecond train [as shown by the solid green curve in Fig. 3(a)]. It should be noticed in the inset of Fig. 5(a) that we can clearly see one branch of considerable intensity of the radiation at the ionization time 0.044 o.c. corresponding to the 240th order harmonic (between the two peaks A and B). This is useful for producing an isolated attosecond pulse [as shown by the dotted red curve in Fig. 3(a)]. Figure 5(b) shows the time-frequency analysis when the initial state is prepared in the coherent superposition of the ground and excited states. As shown in Fig. 5(b), there are three photon-energy peaks, which are labeled as A, B, and C. The maximum harmonic orders of A, B, and C are about 174, 336, and 171, respectively. Peak C is weaker than A and its contribution to the HHG can be ignored. However, in the range of the peak labeled as A, there are at least four quantum paths with two dominant quantum paths which form the first plateau. Thus, for the harmonics in the first plateau, the emission times of these two paths are very different, and the harmonics are not in the same phase. In the range of the peak labeled as B, there is one dominant quantum path and the second plateau is formed (174th-336th). The short quantum path is suppressed and only the long quantum path is left. Thus the harmonics higher than 174th order form a supercontinuum spectrum with a bandwidth of about 251 eV, which is consistent with the solid black curve in Fig. 1(a). The inspection of Fig. 5(b), similar to what we did in the previous section [Fig. 5(a)], reveals that for the harmonics between 174th and 238th order in the second plateau due to the second recollision of the electron with its parent ion, the second short quantum path almost makes a considerable fixed contribution [inset of Fig. 5(b)]. Therefore, the superposition of these harmonics will result in three radiation bursts. Clearly, the contribution of the long quantum path due to the first recollision is higher than that of the short quantum path due to the second recollision. These results agree well with the temporal profile in Figs. 3(b) and 4(a), in which the strong 49-as pulse originates mainly from the contribution of the long quantum path due to the first recollision. By comparing Figs. 5(a) and 5(b), we find that the quantum paths distribution from the case of the ground state is changed by preparing the initial state in a coherent superposition of the ground and excited states. The intensity of peaks A, B, and C in Fig. 5(b) are higher by about three, four, and two orders of magnitude, respectively, than that presented in Fig. 5(a), which explains why the efficiency of the harmonic spectrum is higher in the solid black curve in Fig. 1(a) than in the dotted blue curve in Fig. 1(a). These results indicate that the long quantum path can

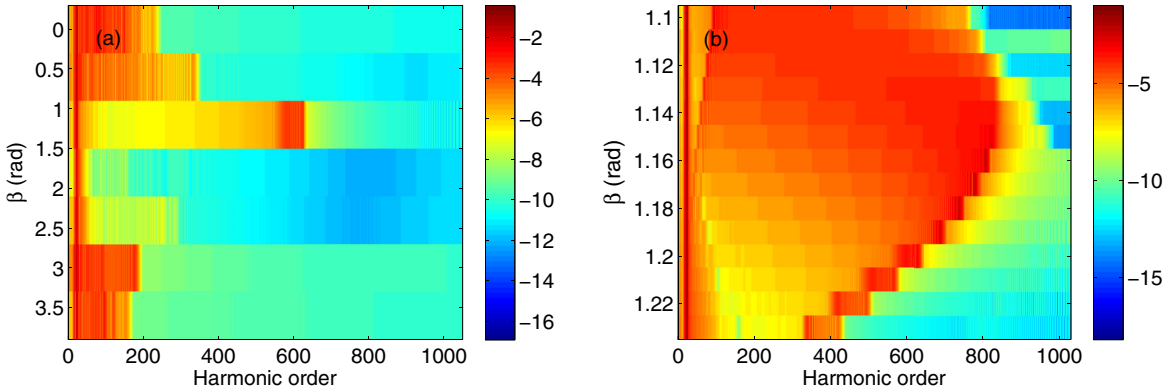

FIG. 6. (Color online) Photon energies from He^+ ions in the coherent superposition state when the β parameter changes (a) from 0 to 3.6 per 0.6 and (b) from 1.10 to 1.23 in each 0.01.

be enhanced by introducing chirping in the preexcited scheme and reveal that the case of the superposition state significantly shortens the duration of the isolated as pulse [the curve in Fig. 4(a)] and enhances the pulse intensity by about six orders of magnitude in comparison with the case of the ground state [dotted red curve in Fig. 3(a)].

According to the above results, to produce broader supercontinuum harmonics photons with high conversion efficiency, the chirp parameters must be optimized in a preexcited scheme. In the following, by changing the β parameter, the harmonic spectrum dependence on time-varying CEP is investigated by fixing τ_0. Figure 6(a) is a three-dimensional graph in which the color represents the intensity of the harmonics, which is the function of the harmonic order and the β parameter. In the simulation, the β parameter changes from 0 to 3.6 per 0.6 and the initial state is prepared as the coherent superposition state. More significantly, the cutoff position for the $\beta = 1.2$ case is obviously extended, compared with the other cases. The optimal supercontinuum extension can be achieved by accurately adjusting β around the $\beta = 1.2$ value. Figure 6(b) shows the HHG power spectra when the β parameter changes from 1.10 to 1.23 per 0.01.

It can be seen that the most distant cutoff of 876 is achieved when the β is set to be 1.14. Figure 7(a) shows the HHG power spectra under the synthesized laser field where the chirp parameter β is chosen to be 1.12 (dashed red curve), 1.14 (solid blue curve), and 1.16 (dot-dashed green curve). As shown by Fig. 7(a), the intense supercontinuum of the HHG spectrum for the $\beta = 1.14$ case is markedly extended, compared to the other cases. When the β parameter changes from 1.14 to 1.12, the supercontinuum width decreases, while the first cutoff shifts to the higher order. Moreover, the lower-order harmonics efficiency increases by reducing the β parameter from 1.14 to 1.12, while the higher-order harmonics efficiency decreases. We can see clearly that with the increasing of the β parameter from 1.14 to 1.16, not only does the maximum harmonic energy keep decreasing, but also the interference structure is seen near the cutoff. Thus, the $\beta = 1.14$ case is an optimum condition covering an intense 1172-eV supercontinuum bandwidth, which is useful in the generation of an intense isolated attosecond pulse. In order to compare, we also show the harmonic spectrum from He^+ ions in the ground state with $\beta = 1.14$ by the dotted black curve in Fig. 7(a). One can clearly see that the harmonic

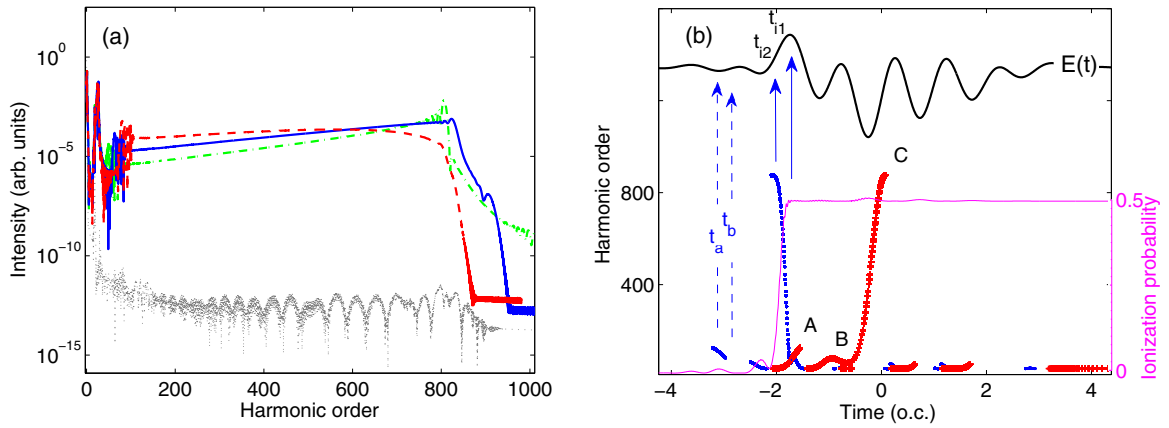

FIG. 7. (Color online) (a) Harmonic spectra from He^+ ions initially prepared in the coherent superposition of the ground and excited states, which correspond to three β parameters, 1.12 (dashed red curve), 1.14 (solid blue curve), and 1.16 (dot-dashed green curve), and initially prepared in the ground state (dotted black curve). (b) Dependence of harmonic order on the ionization time (blue circles) and the emission time (red plus signs) in the synthesized laser field ($\beta = 1.14$, solid black curve), and the corresponding ionization probability (solid magenta curve) for the solid blue curve in (a).

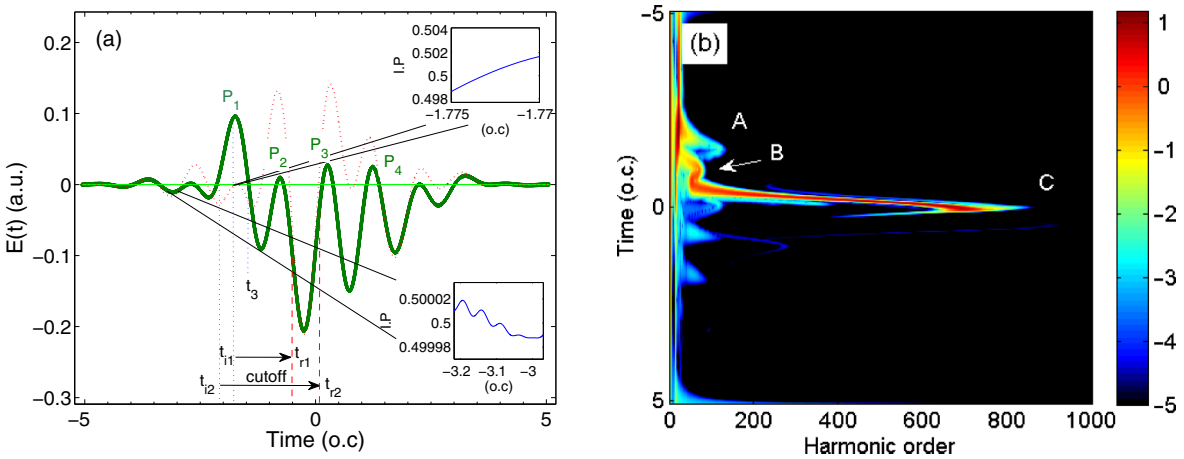

FIG. 8. (Color online) (a) Electric fields of the synthesized pulse with $\beta = 0.58$ (dotted orange curve) and $\beta = 1.14$ (solid green curve). Insets: The ionization probability (I.P.) when He^+ ions are initially prepared as a coherent superposition in the time intervals ranging from -1.775 to -1.770 o.c. (upper inset) and -3.218 to -2.970 o.c. (lower inset). (b) Time-frequency distribution of HHG corresponding to the solid blue curve in Fig. 7(a).

yields for the superposition state case (solid blue curve) enhances by about eight orders of magnitude in comparison with the case of the ground state (dotted black curve) and, in particular, the depth of plateau modulation decreases. In the following, we consider the case of $\beta = 1.14$ for a preexcited system. The corresponding dependence of the harmonic orders (kinetic-energy map) on the ionization and emission times for the $\beta = 1.14$ case is shown in Fig. 7(b). We also show the ionization probability in the optimized laser field (solid black curve) by the solid magenta curve in Fig. 7(b).

This kinetic-energy map displays three main peaks A, B, and C (two main bursts A and B-C) with the maximal harmonic orders of 125, 79, and 876, respectively. As shown in Fig. 7(b), the electric field and ionization rate [the bottom inset of Fig. 8(a)] in the time range from -3.218 (corresponding to 125 H) to -2.970 o.c. (corresponding to 85 H) with the maximum ionization probability of 0.012 are too weak compared to the electric field and ionization rate [the top inset of Fig. 8(a)] in the time range from -1.770 to -1.775 o.c. with the maximum ionization probability of 0.5. Thus, the latter time gate is only the time interval that mainly contributes to harmonics from the 85th to the 125th order, i.e., the burst B-C [Fig. 7(b)]. As a result, there is no continuum plateau produced below the 79th order harmonic because of the interference between peaks C and B, while only peak C contributes to the harmonic spectrum above the 79th order harmonic which shapes a broad soft x-ray continuum plateau of 1235 eV (797 harmonics). We can obviously see that only the time distribution of the electron energies for the short trajectory, which contribute to the supercontinuum spectrum from the 79th to the 876th order, exists. At the ionization time $t_{i2} = -2.055$ o.c. with an ionization probability of 0.055 corresponding to the harmonic photon with maximum energy of $I_p + 1357$ eV (I_p is the ionization potential of the ground state), the ionization probability increases sharply to 0.496 at the ionization time $t_{i1} = -1.751$ o.c. and then is fixed at 0.5. Furthermore, the ionization rate in the time range from the t_{i2} to t_{i1} is very fast compared to the other cases and the main contribution of ionization occurs in this time gate. The supercontinuous harmonics originate from the electrons ionized in the time range from the t_{i2} to t_{i1}. This means that the ionization time gate for the generation of the supercontinuous harmonics and the time gate to have the highest ionization rate occur at the same time in the preexcited scheme. This fact demonstrates the high conversion efficiency of the broadband soft x-ray supercontinuum which can be achieved by this optimum chirp rate. To more clearly understand how an adjusting chirp parameter affects the electron trajectories, we focus on the electric field, as shown in Fig. 8(a). At time $t_{r1} = -0.502$ o.c., the 82nd harmonic is emitted by the electron which is born at the time $t_{i1} = -1.751$ o.c. The 876th harmonic emission (cutoff) occurs at $t_{r2} = 0.061$ o.c. after about two cycles after the ionization of the electron at $t_{i2} = -2.055$ o.c. Thus, the supercontinuous harmonics from the 82nd to the 876th order, which are originated from the short path, are emitted at least after one cycle delay. This means that only the electrons that are born at the part of the time interval that ranges from t_{i2} to t_{i1} at peak P_1 can have the chance of energetic returning to the core with the field reversion, otherwise returning to the core and recombination emission do not happen. For example, the electrons which are born at t_{r1} and t_{r2} never return to the parent ion and, as a result, harmonic photons are not emitted. Therefore, the supercontinuum spectrum is not disturbed. It is clear that for returning the photoelectrons to the vicinity of the parent ion in the presence of a driving pulse, the sign of the electric field must be changed at least once. According to Fig. 7(b), the emission of harmonics higher than the 79th order (the supercontinuous harmonics in the main burst) by the electrons that ionized at field peaks P_2, P_3, and P_4 [as shown in Fig. 8(a)] is prevented because the strength of the mentioned field peaks is so weak that they cannot supply the long time. As a result of the above discussion, the behavior of a multicycle pulse is similar to that of a few-cycle pulse because the optimized laser field delays the recombination time of the ionized electrons by an effective reduction in the sign changing of the driving laser field. So, the high-harmonics emission of the adjacent peaks will obviously be blocked. We also note that the extension of

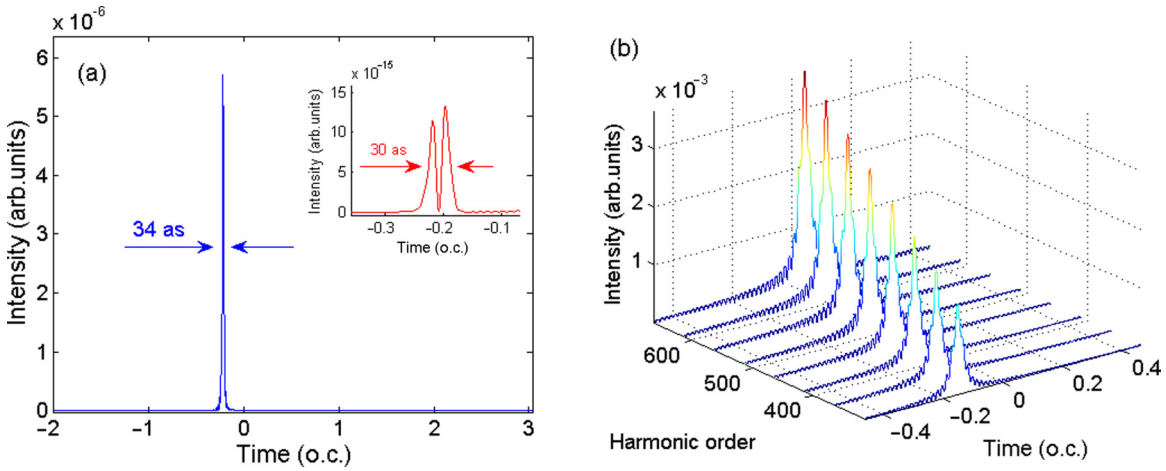

FIG. 9. (Color online) The temporal profiles of the attosecond pulse without any phase compensation from He^+ ions in the coherent superposition state: (a) by superposing the harmonics from the 186th to 239th order and (b) by the harmonics with different central frequencies with a total bandwidth of 82 eV, which corresponds to the solid blue curve in Fig. 7(a). The inset in (a) shows the temporal profile of the attosecond pulse from He^+ ions in the ground state by superposing the harmonics from the 186th to 239th order, which corresponds to the dotted black curve in Fig. 7(a).

the HHG cutoff position by the case of $\beta = 1.14$ is much longer than that of the case of $\beta = 0.58$ because, for the case of $\beta = 0.58$, the cutoff electrons could not receive a higher field to gain more acceleration toward the parent ion. Thus, this causes the electron to acquire low returning kinetic energy and emission of lower photon energy. In order to confirm the above analyses about the redistribution of trajectories, we also illustrate the corresponding time-frequency distributions of HHG in the case of $\beta = 1.14$ in Fig. 8(b). In agreement with the kinetic-energy map in Fig. 7(b), the time-frequency map displays three peaks, i.e., *A*, *B*, and *C*. The maximum harmonic orders of photon-energy peaks *A*, *B*, and *C* are about 125, 79, and 876, respectively. The intensity of peak *C* is the strongest among the three peaks, and the intensity of peak *A* is the weakest one. Furthermore, for the harmonics belong to the intense burst of *C*, the contribution of the long quantum path is greatly suppressed. So, the short quantum path is selected which contributes to the broadband xuv supercontinuum plateau. Clearly, all of these results are consistent with those calculated by the use of the semiclassical three-step model, which was shown in Fig. 7(b). Next, we investigate the attosecond pulse generation. By properly filtering the harmonics from the 409th to the 487th order, an intense isolated pulse of 34 as (the shortest pulse) has been straightforwardly obtained without any phase compensation, as shown in Fig. 9(a). One can see that the temporal profile of the obtained intense attosecond pulse has a clean structure. Moreover, the inset in Fig. 9(a) shows the temporal profile of two adjacent attosecond bursts which are obtained from the ground-state case. The intensity of the isolated attosecond pulse from the case of the superposition state is increased by about eight orders of magnitude in comparison with the case of the ground state. To achieve a realizable bandpass filter, we can utilize an arbitrary filter that selects a bandwidth around an arbitrary photon energy at spectrum. A bandpass filter, which selects a spectrum centered at various values with a total bandwidth of 82 eV, can be proposed, as shown by Fig. 9(b). The durations of the intense single attosecond pulses are below 50 as without any phase compensation and the intensity of the isolated attosecond pulse decreases with the decrease of central frequency. Figure 10 clearly shows that by superposing the total supercontinuum region with phase compensation, we can obtain the shortest 2.7-as intense isolated pulse. In addition, from the inset in Fig. 10, we can see that by superposing harmonics from the 125th to 650th order with phase compensation, we can obtain the 3.7-as intense isolated pulse.

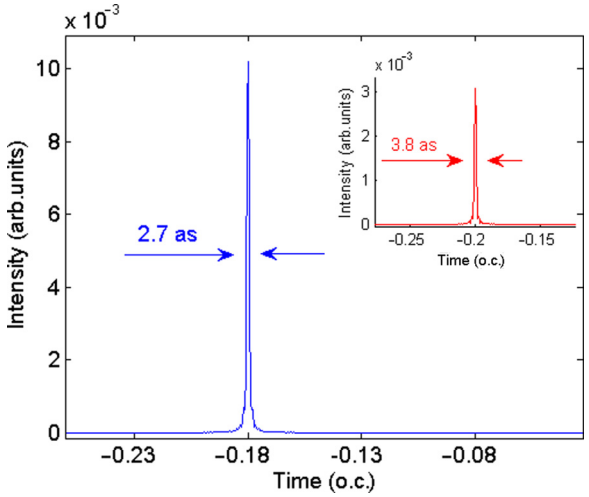

FIG. 10. (Color online) The temporal profiles of the attosecond pulse with phase compensation from He^+ ions in the coherent superposition state: by superposing the total supercontinuum region (solid blue curve) and by the harmonics from the 125th to 650th order (inset). The laser parameters are the same as those in Fig. 7(b).

IV. SUMMARY

In summary, we offer an efficient method to produce a short and intense isolated ultrabroadband attosecond pulse by optimizing the wave form, which consists of a chirped fundamental wave and a chirp-free wave. The model atom

exposed to the combined laser field is chosen to be the He^+ ion which is prepared in a coherent superposition of the ground and excited states. The modulation of the spectral and temporal structures of HHG can be controlled by properly adjusting the chirp parameter, which is explained by the semiclassical three-step model and the calculation of the ionization probability. These results provide complementary and consistent information with the quantum time-frequency analysis concerning the mechanisms for the quantum path selection and supercontinuum expansion. Our numerical results indicate that a quantum path can be enhanced by introducing the chirp in the driving pulse when the He^+ ion is in the preexcited state. So, the duration of the isolated as pulse is significantly shortened and enhances the pulse intensity in comparison with the case of the ground state. By reducing the number of changes in an effective field sign, the electron flight time can be controlled and the high-harmonics emission of the adjacent peaks will be obviously blocked. On the other hand, these factors cause a multipulse behavior similar to a few-cycle pulse. In another point of view, by optimizing the chirp parameter, the recombination time is delayed. Delay of the recombination time permits the electron to sense the larger electric field. Thus, it causes acquisition of the high returning kinetic energy and emission of the higher photon energy. As a result of synchronizing the time to the efficient ionization and the time to produce the higher-order harmonics, the generation of a super strong and broadband supercontinuum with a 1172-eV bandwidth can be successfully accreted in the preexcited scheme. By properly filtering the harmonics, an intense isolated pulse of 34 as (the shortest pulse) with clean time structure can be straightforwardly obtained. Calculations clearly show that by superposing the total supercontinuum region with phase compensation, we can obtain the shortest 3.8-as intense isolated pulse. An efficient sub-39-as isolated attosecond pulse can be straightforwardly achieved by filtering some harmonics with arbitrary central frequencies. This means that the pulse duration is insensitive to the position of the central frequency and in a wide range of harmonics we can obtain a short isolated as pulse without CEP stabilization.

[1] M. Hentschel, R. Kienberger, Ch. Spielmann, G. A. Reider, N. Milosevic, T. Brabec, P. Corkum, U. Heinzmann, M. Drescher, and F. Krausz, Nature (London) **414**, 509 (2001).

[2] G. Mourou and T. Tajima, Science **331**, 41 (2011).

[3] M. Uiberacker, T. Uphues, M. Schultze, A. J. Verhoef, V. Yakovlev, M. F. Kling, J. Rauschenberger, N. M. Kabachnik, H. Schroder, M. Lezius, K. L. Kompa, H. G. Muller, M. J. J. Vrakking, S. Hendel, U. Kleineberg, U. Heinzmann, M. Drescher, and F. Krausz, Nature (London) **446**, 627 (2007).

[4] P. B. Corkum and F. Krausz, Nat. Phys. **3**, 381 (2007).

[5] M. Drescher, M. Hentschel, R. Kienberger, M. Uiberacker, V. Yakovlev, A. Scrinzi, T. Westerwalbesloh, U. Kleineberg, U. Heinzmann, and F. Krausz, Nature (London) **419**, 803 (2002).

[6] R. Kienberger, E. Goulielmakis, M. Uiberacker, A. Baltuska, V. Yakovlev, F. Bammer, A. Scrinzi, T. Westerwalbesloh, U. Kleineberg, U. Heinzmann, M. Drescher, and F. Krausz, Nature (London) **427**, 817 (2004).

[7] P. M. Paul, E. S. Toma, P. Breger, G. Mullot, F. Augé, Ph. Balcou, H. G. Muller, and P. Agostini, Science **292**, 1689 (2001).

[8] Y. Mairesse, A. de Bohan, L. J. Frasinski, H. Merdji, L. C. Dinu, P. Monchicourt, P. Breger, M. Kovacev, T. Auguste, B. Carre, H. G. Muller, P. Agostini, and P. Salières, Phys. Rev. Lett. **93**, 163901 (2004).

[9] Y. Yu, J. Xu, Y. Fu, H. Xiong, H. Xu, J. Yao, B. Zeng, W. Chu, J. Chen, Y. Cheng, and Z. Xu, Phys. Rev. A **80**, 053423 (2009).

[10] H. Du, H. Wang, and B. Hu, Phys. Rev. A **81**, 063813 (2010).

[11] R. Lu, H. He, Y. Guo, and K. Han, J. Phys. B: At. Mol. Opt. Phys. **42**, 225601 (2009).

[12] P. B. Corkum, Phys. Rev. Lett. **71**, 1994 (1993).

[13] M. Lewenstein, P. Balcou, M. Y. Ivanov, A. L'Huillier, and P. B. Corkum, Phys. Rev. A **49**, 2117 (1994).

[14] F. Krausz and M. Ivanov, Rev. Mod. Phys. **81**, 163 (2009).

[15] I.-Lin Liu, P.-C. Li, and Shih-I. Chu, Phys. Rev. A **84**, 033414 (2011).

[16] J. G. Chen, S. L. Zeng, and Y. J. Yang, Phys. Rev. A **82**, 043401 (2010).

[17] Y. Niu, Y. Xiang, Y. Qi, and S. Gong, Phys. Rev. A **80**, 063818 (2009).

[18] S. H. Hekmatara, M. Mohebbi, and J. Rahpeyma, R. Soc. Chem. Adv. **4**, 59064 (2014).

[19] M. Mohebbi, Optik **125**, 3818 (2014).

[20] J. Xu, B. Zeng, and Y. Yu, Phys. Rev. A **82**, 053822 (2010).

[21] M. Mohebbi and S. Batebi, Chin. Opt. Lett. **10**, 081901 (2012).

[22] Z. Chang, Phys. Rev. A **71**, 023813 (2005).

[23] X. Feng, S. Gilbertson, H. Mashiko, H. Wang, S. D. Khan, M. Chini, Y. Wu, K. Zhao, and Z. Chang, Phys. Rev. Lett. **103**, 183901 (2009).

[24] G. T. Zhang, J. Wu, C. L. Xia, and X. S. Liu, Phys. Rev. A **80**, 055404 (2009).

[25] H. K. Avetissian and G. F. Mkrtchian, Phys. Rev. A **66**, 033403 (2002).

[26] H. K. Avetissian, B. R. Avchyan, and G. F. Mkrtchian, Phys. Rev. A **77**, 023409 (2008).

[27] H. K. Avetissian, B. R. Avchyan, and G. F. Mkrtchian, J. Phys. B **45**, 025402 (2012).

[28] J. B. Watson, A. Sanpera, X. Chen, and K. Burnett, Phys. Rev. A **53**, R1962 (1996).

[29] F. I. Gauthey, C. H. Keitel, P. L. Knight, and A. Maquet, Phys. Rev. A **52**, 525 (1995).

[30] J. G. Chen, Y. J. Yang, S. L. Zeng, and H. Q. Liang, Phys. Rev. A **83**, 023401 (2011).

[31] M. Mohebbi and S. Batebi, Opt. Commun. **296**, 113 (2013).

[32] K. Ishikawa, Phys. Rev. Lett. **91**, 043002 (2003).

[33] S. Zhdanovich, E. A. Shapiro, J. W. Hepburn, M. Shapiro, and V. Milner, Phys. Rev. A **80**, 063405 (2009).

[34] X. Yang and S. Zhu, Phys. Rev. A **78**, 023818 (2008).

[35] B. Y. Chang, I. R. Solá, V. S. Malinovsky, and J. Santamaría, Phys. Rev. A **64**, 033420 (2001).

[36] X. Yang, Z. Sun, and Z. Wang, Phys. Rev. A **76**, 043417 (2007).

[37] B. Wang, T. Cheng, X. Li, P. Fu, S. Chen, and J. Liu, Phys. Rev. A **72**, 063412 (2005).

[38] W. Hong, Q. Zhang, X. Zhu, and P. Lu, Opt. Express **19**, 4728 (2011).
[39] J. Luo, Y. Li, Z. Wang, Q. Zhang, P. Lan, and P. Lu, J. Opt. Soc. Am. B **30**, 2469 (2013).
[40] E. A. Gibson, A. Paul, N. Wagner, R. Tobey, S. Backus, I. P. Christov, M. M. Murnane, and H. C. Kapteyn, Phys. Rev. Lett. **92**, 033001 (2004).
[41] A. Sanpera, J. B. Watson, M. Lewenstein, and K. Burnett, Phys. Rev. A **54**, 4320 (1996).
[42] E. Takahashi, Y. Nabekawa, T. Otsuka, M. Obara, and K. Midorikawa, Phys. Rev. A **66**, 021802 (2002).
[43] X. M. Tong and Shih-I. Chu, Phys. Rev. A **61**, 021802(R) (2000).
[44] J. T. Lin, D. S. Chuu, and T. F. Jiang, Phys. Rev. A **58**, 2337 (1998).
[45] Z. Chang, A. Rundquist, H. Wang, I. Christov, H. C. Kapteyn, and M. M. Murnane, Phys. Rev. A **58**, R30(R) (1998).
[46] J. T. Lin and T. F. Jiang, J. Phys. B **32**, 4001 (1999).
[47] M. Mohebbi and S. Batebi, J. Electron Spectrosc. Rel. Phenom. **185**, 578 (2012).
[48] Y. Mairesse, A. de Bohan, L. J. Frasinski, H. Merdji, L. C. Dinu, P. Monchicourt, P. Breger, M. Kovacev, R. Taeb, B. Carré, H. G. Muller, P. Agostini, and P. Salires, Science **302**, 1540 (2003).
[49] G. T. Zhang and X. S. Liu, J. Phys. B: At. Mol. Opt. Phys. **42**, 125603 (2009).